

Supplementary information to Principles of hydrodynamic particle manipulation in internal Stokes flow

Xuchen Liu, Partha Kumar Das, and Sascha Hilgenfeldt
Department of Mechanical Science and Engineering,
University of Illinois at Urbana-Champaign, Urbana, IL 61801, USA

September 11, 2024

Alternative modeling with a no-stress boundary

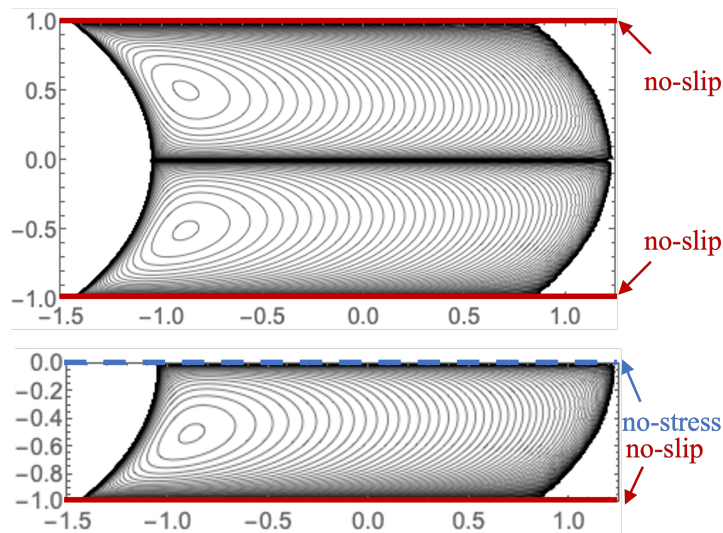


Figure 1: Different boundary conditions imposed for the Moffatt eddy flow field. Top: no-slip BCs at $y = -1$ and $y = +1$. Bottom: noslip BC at $y = -1$ and no-stress BC at $y = 0$.

In this work, we have focused on particles seeded in the lower half of the channel, being transported in a vortex bounded by the lines $y = -1$ (lower wall) and $y = 0$, in a channel spanning twice that width to a second no-slip wall at $y = +1$ (see the upper panel of Fig 1). It is tempting to instead simplify the problem by taking as the modeling

domain only the lower half of the channel to start with, while modeling the boundary at $y = 0$ as a stress-free boundary (this property is true for the background flow and follows from symmetry). The lower panel of Fig 1 shows this scenario.

The influence of a nearby no-stress boundary on the wall-normal velocity of a spherical particle in an arbitrary Stokes flow was quantified in Rallabandi *et al.* (2017) alongside the results for a no-slip wall. The only difference between these two cases is that the hydrodynamic resistances in the formulae for the velocity correction \mathbf{W} have different functional forms, which we denote \mathcal{A}_{II} , \mathcal{B}_{II} , \mathcal{C}_{II} and \mathcal{D}_{II} . In the following, we will exclusively look at particle trajectories with large Δ with respect to any wall. The asymptotic expressions for the no-stress resistances at $\Delta \gg 1$ are

$$\mathcal{A}_{II,large} \approx 1 + \frac{3}{4}\Delta^{-1} \quad (1)$$

$$\mathcal{B}_{II,large} \approx \frac{5}{8}\Delta^{-2} \quad (2)$$

$$\mathcal{C}_{II,large} \approx \frac{7}{16}\Delta^{-3} \quad (3)$$

$$\mathcal{D}_{II,large} \approx \frac{1}{3} + \frac{1}{4}\Delta^{-1} \quad (4)$$

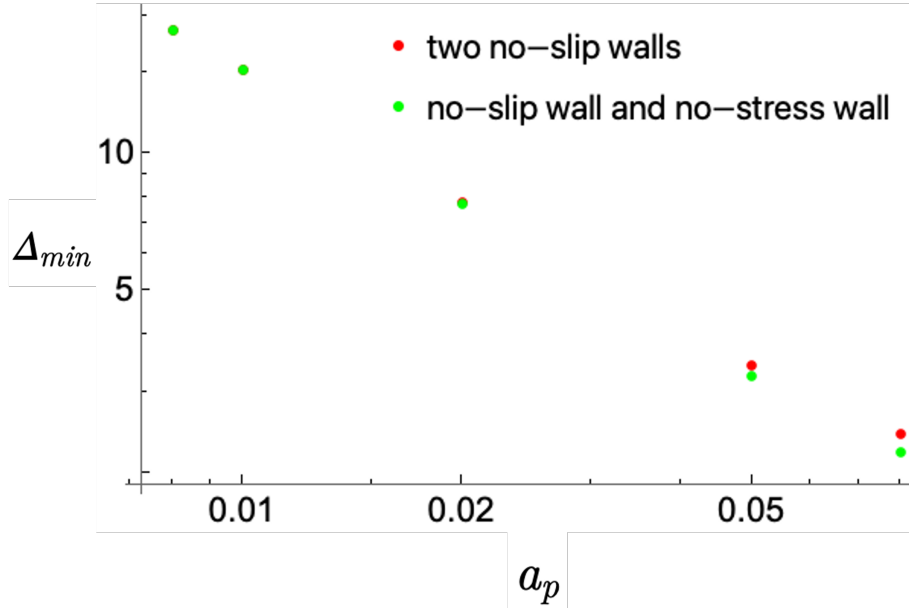


Figure 2: Non-dimensional minimum gap Δ_{min} between particle and wall on stable limit cycle trajectories, for both boundary condition scenarios depicted in Fig. 1. Results are indistinguishable for $a_p \lesssim 0.02$.

We use equation (2.10) from the main text with these expressions as well as the no-slip expressions (\mathcal{A}_{large} , \mathcal{B}_{large} , \mathcal{C}_{large} and \mathcal{D}_{large}) with respect to the $y = -1$ wall to solve for stable limit cycles. By varying particle sizes, we compare their closest distances to the wall with those stable limit cycles calculated for the scenario with two no-slip walls (Fig 2). The two calculations are indistinguishable up to $a_p = 0.02$, but noticeable differences appear for somewhat larger particles.

Note that the disturbance flow due to the presence of the particle modifies the background flow in such a way that $y = 0$ is *not* a strict line of symmetry anymore, and the no-stress boundary condition is not strictly applicable. In contrast, the no-slip boundaries at $y = \pm 1$ remain unchanged. As a_p increases, the effect of the disturbance flow of the particle becomes more and more important, and the violation of the no-stress boundary condition becomes more pronounced. Thus, the simplified no-slip/no-stress approach should not be used for particles of even moderate size ($a_p \gtrsim 0.05$), while the no-slip/no-slip scenario remains physical.

Calculation of limit cycles with uncertainty bandwidths

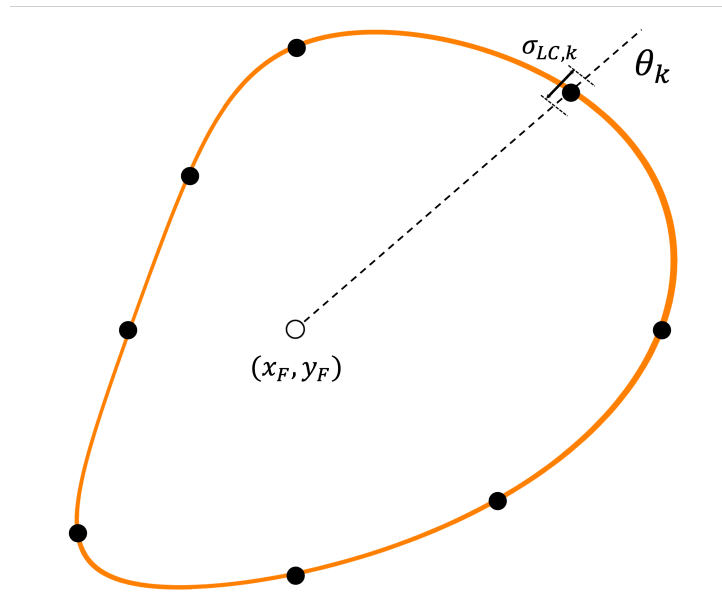


Figure 3: An exemplary limit cycle ($a_p = 0.1$) with eight different angles θ_k . Each angle is used as the initial condition for further limit cycle computations, resulting in quantifications of uncertainty bandwidths.

Using a polar coordinate system with the origin at the Faxen field vortex center (x_F, y_F) , we choose eight different fixed angles θ_k (Fig 3). At each θ_k , we collect the radial coordinates of limit cycles computed from N different initial conditions,

obtaining the mean and standard deviation of these radial positions in the usual way,

$$\frac{1}{N} \sum_{i=1}^N r_{LC}(\theta_k, \mathbf{x}_{0,i}) = \bar{r}_{LC,k}, \quad (5)$$

$$\sqrt{\left(\frac{1}{N} \sum_{i=1}^N (r_{LC}(\theta_k, \mathbf{x}_{0,i}) - \bar{r}_{LC,k})^2 \right)} = \sigma_{LC,k} \quad (6)$$

We take $\sigma_{LC,k}$ as a quantitative measure of the bandwidth of the limit cycle at angle θ_k (for a given particle size). The bandwidths change with θ_k (but remain within the same order of magnitude). In the main text, we focus on $\theta_k = -\pi/2$, to estimate the error in the closest approach of the particle to the wall. We find that this error grows as a_p decreases and becomes too large to distinguish the wall approach distance of the limit cycles for $a_p = 0.008$ and $a_p = 0.005$.

References

RALLABANDI, BHARGAV, HILGENFELDT, SASCHA & STONE, HOWARD A 2017 Hydrodynamic force on a sphere normal to an obstacle due to a non-uniform flow. *Journal of Fluid Mechanics* **818**, 407–434.